Tuning the thermal conductivity of Si membrane using nanopillars: from crystalline to amorphous pillars

Lina Yang[1*], Yixin Xu[2], Xianheng Wang[1], Yanguang Zhou[2,3*]

[1] School of Aerospace Engineering, Beijing Institute of Technology, Beijing 100081, China

[2] Department of Mechanical and Aerospace Engineering, The Hong Kong University of Science and Technology, Clear Water Bay, Kowloon, Hong Kong Special Administrative Region

[3] HKUST Shenzhen-Hong Kong Collaborative Innovation Research Institute, Futian, Shenzhen, Guangdong, China

Email: yangln@bit.edu.cn (L. Yang); maeygzhou@ust.hk (Y. Zhou)

Abstract

Tuning thermal transport in nanostructures is essential for many applications, such as thermal management and thermoelectrics. Nanophononic metamaterials (NPM) have shown great potential for reducing thermal conductivity by introducing local resonant hybridization. In this work, the thermal conductivity of NPM with crystalline Si (c-Si) pillar, crystalline Ge (c-Ge) pillar and amorphous Si (a-Si) pillar are systematically investigated by molecular dynamics method. The analyses of phonon dispersion and spectral energy density show that phonon dispersions of Si membrane are flattened due to local resonant hybridization induced by both crystalline and amorphous pillar. In addition, a-Si pillar can cause larger reduction of thermal conductivity compared with c-Si pillar. Specifically, when increasing the atomic mass of atoms in pillars, the thermal conductivity of NPMs with crystalline pillar is increased because of the weakened phonon hybridization, however, the thermal conductivity of NPMs with amorphous pillar is almost unchanged, which indicates that the phonon transports are mainly affected by the scatterings at the interface between amorphous pillar and Si membrane. The results of this work can provide meaningful insights on controlling thermal transport in NPMs by choosing the materials and atomic mass of pillars for specific applications.

Keywords: Thermal conductivity, nanophononic metamaterial, phonon hybridization, molecular dynamics simulation.

1. Introduction

Controlling thermal transport in nanostructures has attracted significant attention in recent years due to its promising applications such as thermal management[1,2] and thermoelectric energy conversion[3-5]. For instance, in the pursuit of high-efficiency thermoelectrics, a promising avenue of the strategies lies in the development of nanophononic metamaterials (NPM) with low thermal conductivity (κ).[6-8] NPMs enable phonon resonant hybridizations between the vibrational modes of nanoresonators and the phonon modes of the host medium, leading to enhanced control over thermal conductivity.[9-12] Meanwhile, previous studies found the pillared silicon (Si) membrane can reduce the κ by two orders of magnitudes[9,13]. Unlike nanoscale phononic crystals[14,15], NPM does not require periodicity in the arrangement of resonators to achieve resonant hybridizations, which renders NPM highly robust to disorder in the arrangement of resonators[9]. Additionally, as the resonators of NPM are located outside the membrane[7,13,16], electron transport in these materials remains almost unaffected, which is highly desirable for developing high-efficiency thermoelectrics.

Substantial efforts have been aimed at comprehending the thermal transport properties of NPMs and the underlying mechanisms since the NPM was initially proposed by Davis and Hussein in 2014 [6]. For instance, Anufriev et al. found that the κ of nanobeams with aluminum (Al) nanopillar is about 20% smaller compared with the pristine nanobeams, which is mainly caused by phonon scatterings at the pillar/beam interface due to the intermixing of Al and Si atoms[17]. Maire et al. showed that the cross-sections control the κ of nanowires with fishbone nanostructures, and the periodic wings further reduce the κ[18]. Later analyses found that the reduction of κ is mainly caused by the periodicity of wings which can flatten the phonon dispersions, rather than by local resonances[19]. By conducting atomistic modeling and experiments, Neogi et al. found that the reduction of κ in ultrathin suspended silicon membranes is mainly controlled by surface scatterings because the rough layers of native oxide at surfaces limit the mean free path of thermal phonons below 100 nm.[20] Similarly, Huang et al. reported that the κ of suspended silicon membranes with nanopillars is controlled by incoherent phonon scatterings causing less than 16% reduction of κ, which is examined by comparing the results of Monte Carlo simulation and experimental measurements.[21] Recently,

the device-scale suspended silicon membranes with GaN nanopillars were fabricated, and experimental measurements found that the nanopillars cause up to 21% reduction of κ, meanwhile, the power factor remains unaffected[16].

Besides these experimental works, different types of NPMs have been studied theoretically. Xiong et al. found that combining a designed resonant structure with alloying can lead to extremely low κ in Si nanowires, because the local resonances greatly reduce the phonon group velocities and mean free paths in the low frequency (<4 THz) range, concurrently, alloy scatterings impede high frequency phonons.[7] Later, Zhang et al. designed a Si nanowire with helical wall which is more effective on reducing κ compared with straight nanowalls and nanopillars. They demonstrated the resonant hybridization and mode localization in the helical walls by analyzing the phonon dispersions and phonon spatial distributions, respectively.[22] Further, it was found that introducing imperfections such as vacancy defects, mass mismatch, and alloy disorder in the pillars can weaken the local resonant hybridization, leading to a higher κ compared with that of the pristine NPMs[23,24]. For instance, the κ of pillared graphene nanoribbon (GNR) is increased from ~47 W/mK to ~63 W/mK by increasing the atomic mass of atoms in pillars.[23] Although previous works have reported that introducing nanopillars will affect κ through several mechanisms[11] such as local resonance[13], phonon interference due to pillar periodicity[19] and diffuse phonon scatterings[17,20,21], tuning κ of NPMs by designing different kinds of resonators is less investigated, and the corresponding phonon transport behaviors remain unclear.

In this work, the effect of the crystalline Si (c-Si) pillar, amorphous Si (a-Si) pillar and crystalline Ge (c-Ge) pillar on regulating κ of Si membrane is investigated by equilibrium molecular dynamics simulations (EMD). In addition, the mass of atoms in pillars is tuned to manipulate the κ of NPMs with c-Si and a-Si pillars. The phonon local resonant hybridizations in NPMs are systematically analyzed by calculating phonon dispersions and spectral energy distribution (SED). Further, the spectral thermal conductivity is also quantified. The results of our work are expected to provide insights into the interplay between the resonators of NPMs and phonon transport.

2. Model and Method

To study the κ in NPMs, Si membrane with c-Si pillar, c-Ge pillar, and a-Si pillar in Figure 1 (a) are created, which are noted as Type 3, Type 2, and Type 4, respectively. When the atomic mass of atoms in the c-Si pillar is changed to M in amu unit, it is noted as c-Si^M pillar. The NPM with c-Si^M pillar is represented by Type 1. Here, the atomic mass of Si and Ge atoms is denoted by MSi and MGe, respectively. If M equals MSi, the c-Si^M pillar represents the c-Si pillar. In Figure 1 (b) and (c), the value of M is set as MGe for Type 1. $La = 5.431$Å and $L_{Ge} = 5.66$ Å are the lattice constant of bulk Si and Ge, respectively. The unit cell of Si membrane is $6La \times 6La \times 6La$. The size of the c-Ge pillar is $4L_{Ge} \times 4L_{Ge} \times 6L_{Ge}$, and the size of other pillars is $4La \times 4La \times 6La$. The images of the system structures are created with OVITO[25], version 2.9.0, in this paper.
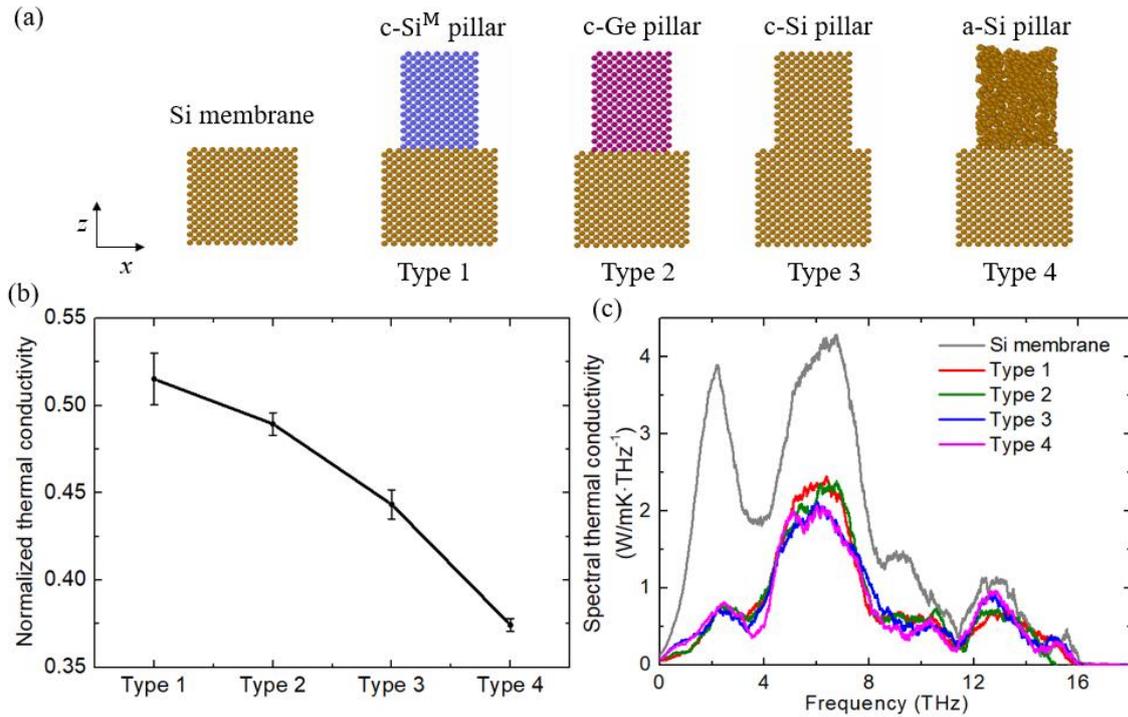
Figure 1. (a) The structure Si membrane, NPM with c-Si^M pillar (Type 1), NPM with c-Ge pillar (Type 2), NPM with c-Si pillar (Type 3) and NPM with a-Si pillar (Type 4). (b) Normalized thermal conductivity of NPM from Type 1 to Type 4. The κ of NPM is normalized by the κ of Si membrane. (c) Spectral thermal conductivity of Si membrane and NPMs versus frequency. In (b) and (c), the value of M is set as MGe for Type 1.

The thermal conductivity of NPM is calculated by EMD method. In the simulations, the periodic boundary condition is applied in the x and y directions, and the free boundary condition is applied in the z direction. Tersoff potential is used to describe the interaction between Si atoms[26] and Ge atoms. The couplings between Si and Ge atoms are obtained by following the combination rule [26], which has been applied to describe the Si and the SiC system. All molecular dynamics simulations are performed using LAMMPS (large-scale atomic/molecular massively parallel simulator)[27], and the temperature is set as 300 K. Thermal conductivity is calculated from the Green-Kubo formula[28],

$$\kappa = \frac{1}{2Vk_BT^2}\int_0^\infty \langle J(0) \cdot J(\tau)\rangle \, d\tau \tag{1}$$

where k_B is the Boltzmann constant, V is the system volume, T is the temperature and J is the heat current. The time step in EMD simulations is set as 0.5 fs. Firstly, the NPM system is equilibrated at 300 K using canonical ensemble with Langevin heat reservoir for 6×10^5 steps (300 ps). Then, the heat current is recorded at each step during the EMD simulations under microcanonical ensemble (NVE) for 8×10^6 steps (4 ns). The final results are averaged over twenty simulations with different initial conditions. The statistical errors are obtained according to the method mentioned in Ref[28].

The a-Si pillar is obtained by the melt-quenching method[29-32]. Initially, the Si membrane with the c-Si pillar is created. The atoms in the Si membrane are fixed, and the atoms in the c-Si pillar are melted at 3600 K by Nosé-Hoover thermostat for 0.5 ns, then the pillar is quickly quenched to 1000 K at the rate of 860 K/ps. Finally, the atoms in the pillar are annealed at 1000 K for 0.5 ns, then quickly quenched to 20 K at the rate of 160 K/ps. To determine the atomic configuration of the a-Si pillar, an equilibration simulation is first performed for the a-Si pillar for 2.5 ns in an NVT ensemble, and then the steady atomic positions are calculated by averaging the time-dependent atomic positions during the next 2.5 ns.

To characterize the phonon transport in NPMs, the phonon dispersions of NPMs and Si membranes are calculated by lattice dynamics (LD) implemented in GULP[33]. The SED[34-36] is obtained directly from the MD simulations by recording the velocities of atoms. The SED expression Φ' is given by

$$\Phi'(k, \omega) = \frac{1}{4\pi\tau_0} \sum_\alpha^3 \sum_{b=1}^n \frac{m_b}{N} \left| \sum_1^N \int_0^{\tau_0} \dot{u}_\alpha(l, b, t) exp\Theta dt \right|^2 \tag{2}$$

where $\dot{u}_\alpha$ is the αth component of the velocity of the bth atom in the lth unit cell at time t, and $\Theta = i[\vec{k} \cdot \vec{r_0}(l, b) - \omega t]$. m_b is the mass of the bth atom. τ_0 is the simulation time, $\vec{r_0}$ is the equilibrium position vector of the lth unit cell, and ω is the angular frequency. Here, the unit of Φ' is J·ps. N is the total number of unit cells, and n is the number of atoms in the unit cell. In the SED analyses, the supercell of NPM consists of 40 unit cells in the x direction and 1 unit cell in the y and z directions. Here, the MD simulations are performed at 300 K for 2×10^6 time steps to extract the atomic velocities.

To quantify the spectral phonon transmission function, we further calculate the spectral thermal conductivity using nonequilibrium molecular dynamics simulations (NEMD), in which the spectral heat current can be calculated by [37,38]

$$Q(\omega) = 2 \sum_{i \in left} \sum_{j \in right} Re \left[\int_{-\infty}^{+\infty} \left\langle \frac{\partial U_j}{\partial \vec{r_i}} \right|_\tau \vec{v}_i(0) - \frac{\partial U_i}{\partial \vec{r_j}} \right|_\tau \vec{v}_j(0) \right\rangle e^{-i\omega\tau} d\tau] \tag{3}$$

where U_j is the potential energy of atom j, $\vec{v}_i$ is the velocity of atom i and $\langle \rangle$ denotes the time average in MD simulations. The atomic velocities $\vec{v}_i$ and the atomic potential partial function $\frac{\partial U_j}{\partial \vec{r_i}}$ are updated every 20 steps, i.e., 10 fs. The size effects and the configuration of NEMD simulations are shown in Figure S7 in the Supplementary Materials. After that, by assuming the same temperature gradient ∇T over all the phonons, the spectral thermal conductivity is then calculated by Fourier's law, i.e., $\kappa(\omega) = Q(\omega)/A\nabla T$ in which A denotes the system cross-section area and ∇T is the temperature gradient along the in-plane direction.

3. Results

3.1 Thermal conductivity of NPMs

The thermal conductivity of NPMs in Figure 1 (a) is calculated by EMD method through Eq.(1). In Figure 2 (b) and (c), the value of M is set as MGe for c-Si^M pillar in Type 1. For comparison, the thermal conductivity of bulk Si and Si membranes in Figure 1 (a) is also computed. The simulation cell of bulk Si is set as $6La \times 6La \times 6La$ with periodic boundary

conditions in all three spatial directions to overcome the size effect[28,39,40]. The calculated κ is 238.4±3.6 W/m-K and 40.6±0.6 W/m-K for bulk Si and Si membrane at 300 K, respectively, which is consistent with the prediction in Ref.[41] and Ref.[20]. The thermal conductivity as a function of time is shown in Figure S1 in the Supplementary Materials. Though the value of κ for bulk Si by MD method deviates from experiment results[42], this discrepancy will not severely affect the comparison of NPMs and Si membrane due to the same MD simulation methods and potential parameters. The κ of NPMs is normalized by the κ of Si membrane, which is shown in Figure 1 (b). The normalized κ of NPM with c-Si^M pillar and c-Ge pillar is larger than that of NPM with c-Si pillar, while a-Si has a stronger effect on the reduction of κ compared c-Si pillar.

To further understand the reduction κ of NPMs in Figure 1 (b), the spectral κ (Figure 1 (c)) is investigated. Compared with the Si membrane, the spectral κ of NPMs is reduced in a wide range of frequencies from 0 to 14 THz. At the low-frequency range (< 2.0 THz), the c-Si^M pillar and the c-Ge pillar cause slightly smaller spectral κ compared with the c-Si pillar. However, from 5 to 7.5 THz, NPMs with c-Si^M pillar and c-Ge pillar have larger spectral κ, which leads to the larger κ compared with NPM with c-Si pillar. Furthermore, the contribution of low-frequency phonons (< 2.0 THz) to spectral κ is almost equivalent in the a-Si pillared NPM and the c-Si pillared NPM. However, the spectral κ of NPM with a-Si pillar is smaller for frequency ranging from 3.5 to 4.5 THz and 7.5 to 10 THz, which leads to the smaller κ compared with NPM with the c-Si pillar.

It was reported that the phonon hybridization between the host medium and the resonant surface structures played an essential role in reducing the thermal conductivity of nanostructures[7,19,24]. Here, the phonon hybridizations in the NPMs are analyzed by calculating their phonon dispersion using the lattice dynamics method implemented in GULP[33], shown in Figure 2 (a). In addition, the SED spectrum of the Si membrane and the Si membrane in NPMs, as shown in Figure 2 (b), are also calculated. The SED spectrum of NPMs considering all atoms in the system is shown in Figure S2 in the Supplementary Material. Because phonon modes with high frequency are difficult to distinguish in the SED spectrum, we only consider the low-frequency phonon modes (≤ 1.5 THz) here. The results show that introducing the nanopillars

can affect the low-frequency phonon modes of Si membrane, for example, the first resonant hybridization causing the flattened bands happens at ~0.1 THz for Type 1 and Type 2 NPMs and at ~0.15 THz for Type 3 and Type 4 NPMs, which leads to a reduction of κ of NPM compared with the pure Si membrane. In addition, the phonon dispersions of Type 1 and Type 3 are close to that of Type 2 and Type 4, respectively. However, the lattice mismatch at the interface between the c-Ge pillar and Si membrane causes stronger phonon scatterings, therefore, NPM with the c-Ge pillar can have a smaller κ than NPM with the c-Si^M pillar. Similarly, the roughness of the amorphous pillar also causes stronger phonon scatterings at the interface between the a-Si pillar and Si membrane, therefore, NPM with the a-Si pillar can have a smaller κ than NPM with the c-Si pillar.
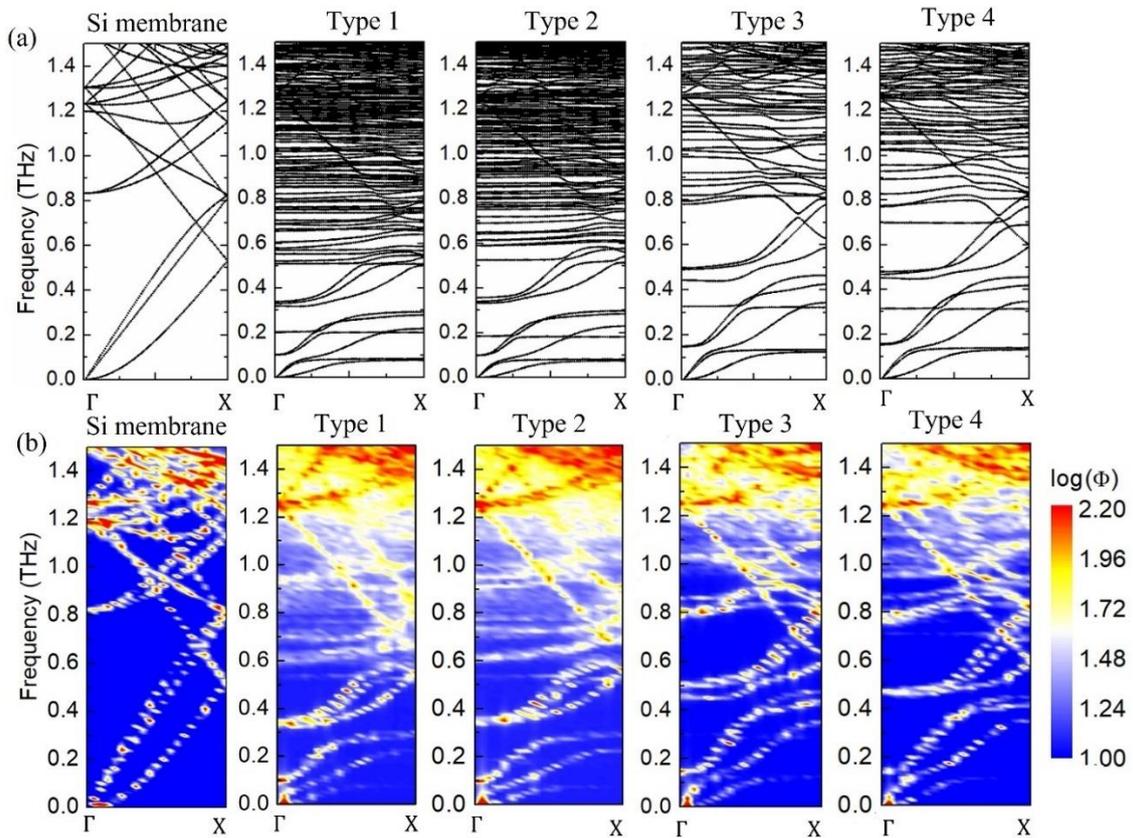
Figure 2 (a) Phonon dispersions of Si membrane and NPMs calculated by lattice dynamics. (b) SED spectrum of Si membrane and NPMs only considering atoms in the Si membrane. The meaning of Type 1 to Type 4 is the same as in Figure 1.

3.2 Phonon hybridization and anomalous thermal conductivity
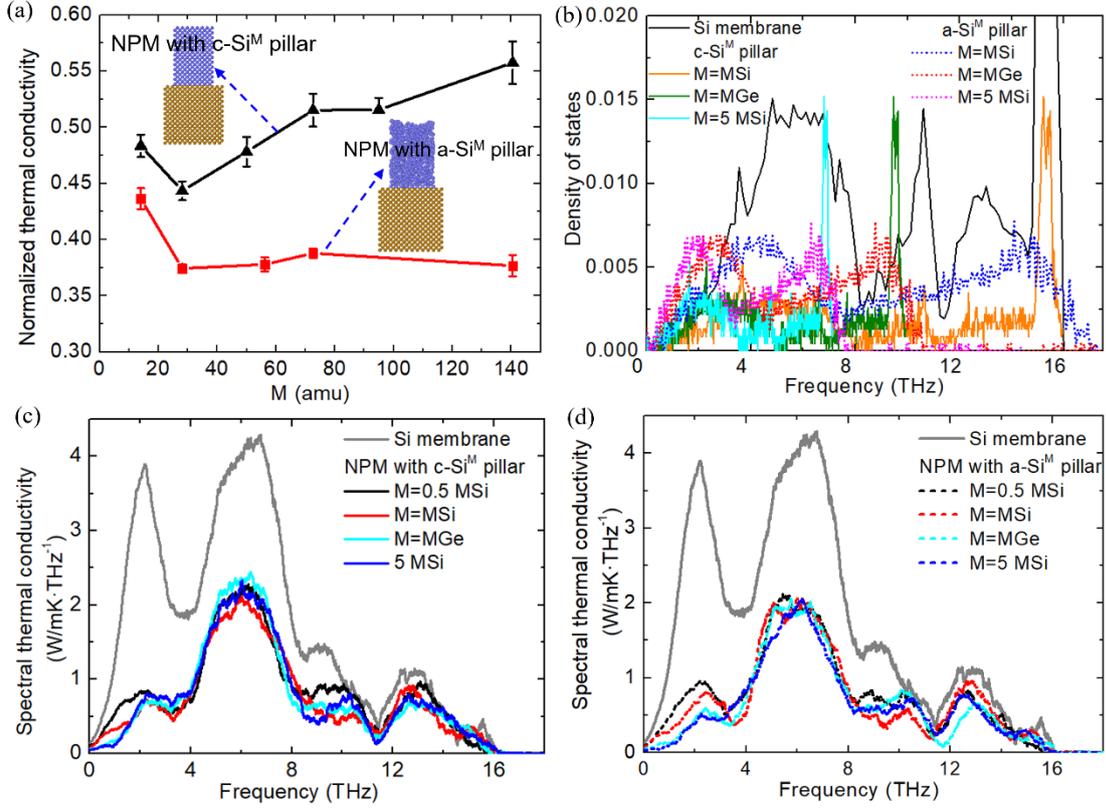
Figure 3 (a) Normalized thermal conductivity of NPM with c-Si^M pillar and a-Si^M pillar versus the value of M. Here, when the atomic mass of atoms in the c-Si is changed to M in amu, it is denoted as a-Si^M pillar. The thermal conductivity of NPM is normalized by κ of the Si membrane. (b) Density of states (DOS) versus frequency for c-Si^M pillar and a-Si^M pillar. (c) Spectral thermal conductivity of NPM with c-Si^M pillar. (d) Spectral thermal conductivity of NPM with a-Si^M pillar.

The frequency of vibrational modes of the pillar can be controlled by varying its atomic mass. Additionally, it was reported that changing the atomic mass of the pillar can also weaken the resonant hybridization and abnormally increase the κ[24]. To further study the effect of the atomic mass, the thermal conductivity of NPM with c-Si^M pillar and a-Si^M pillar is calculated, where the value of M is varied from 0.5 MSi to 5 MSi. Here, when the atomic mass of atoms in the a-Si is changed to M in amu unit, it is denoted as a-Si^M pillar. The thermal conductivity

of NPM is normalized by κ of the Si membrane, which is shown in Figure 3 (a), the κ of NPMs versus time are shown in Figure S3 in the Supplementary Materials. For NPM with the c-Si^M pillar, κ is the smallest when M equals MSi, and largely increased as the M increases from MSi to 5 MSi, which is consistent with the findings of graphene NPM with larger mass pillar.[23,24] Similarly, the NPM with a-Si^M pillar has a larger κ when M is decreased from MSi to 0.5 MSi. However, its κ is almost unchanged as M increases from MSi to 5 MSi. The extreme cases in which the M is set as 5000MSi for NPMs with c-Si^M pillar and a-Si^M pillar are shown in Figure S5 in the Supplementary Materials.

To understand the different behavior of κ between NPM with c-Si^M pillar and a-Si^M pillar as M increases from MSi to 5 MSi, the density of states (DOS) in Figure 3 (b) and spectral κ in Figure 3 (c) and (d) are calculated. Figure 3 (c) shows that for NPM with the c-Si^M pillar, the spectral κ contributed by the low-frequency phonon (<2 THz) is decreased due to the stronger hybridization at the low-frequency as M increases (shown in Figure 4), while, the spectral κ contributed by phonon with frequency from 4.5 to 7.5 THz is increased, leading to the increase of the κ. Figure 3 (d) shows that in NPM with a-Si^M pillar, the spectral κ decreases as M increases for low frequency phonons (< 3.5 THz), and for other frequency ranges, it does not show obvious trends as M increases.

The DOS in Figure 3 (b) shows that the vibrational frequencies of the c-Si^M pillar and a-Si^M pillar are suppressed toward low frequency as M increases. For example, the vibrational modes at ~16 THz are suppressed to ~7 THz when M=5 MSi. Therefore, there will be fewer resonant hybridizations above ~7 THz in the NPM, which means that the frequency range of resonant hybridization is reduced. In addition, changing the atomic mass of the pillar can weaken the resonant hybridizations[24]. Therefore, the κ of NPM with c-Si^M pillar is increased as M increases due to the weakened resonant hybridizations and reduced frequency range of resonant hybridizations. This finding also indicates that the resonant hybridizations dominate the suppression of phonon transport in NPM with c-Si^M pillar, and the phonon scatterings at the interface between c-Si^M pillar and Si membrane do not severely affect the phonon transport. The behavior of resonant hybridization as M increases in NPM with a-Si^M pillar is similar to that in NPM with c-Si^M pillar (shown in Figure 4). However, the κ of NPM with a-Si^M pillar

is almost unchanged as M increases, which implies that the phonon scatterings at the interface between the a-Si^M pillar and the Si membrane dominate the suppression of phonon transport.
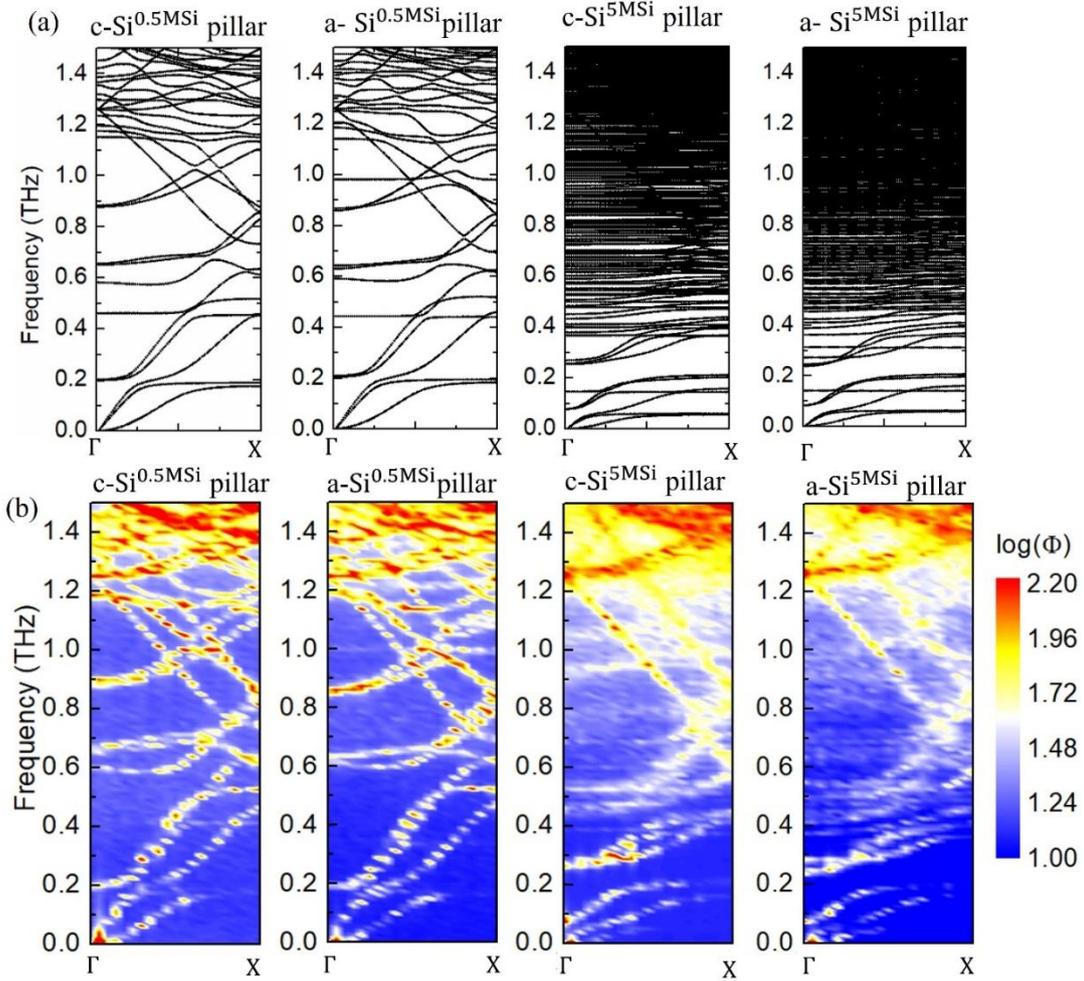
Figure 4 (a) Phonon dispersions of NPMs with c-Si^M pillar and a-Si^M pillar calculated by lattice dynamics. (b) SED spectrum of NPMs with c-Si^M pillar and a-Si^M pillars, in which only the atoms in Si membrane are considered. The value of M is set as 0.5 MSi and 5 MSi to compare the change of phonon dispersions. Here, c-Si$^{0.5MSi}$ and a-Si$^{0.5\ MSi}$ pillar represent c-Si^M and a-Si^M pillar with M=0.5 MSi, and c-Si^{5MSi} and a-Si^{5MSi} pillar represents c-Si^M and a-Si^M pillar with M=5 MSi.

Furthermore, the value of M is set as 0.5 MSi and 5 MSi to compare the change of phonon dispersion of NPMs in Figure 4 (a). Here, the c-Si$^{0.5\ MSi}$ pillar and c-Si$^{5\ MSi}$ pillar represent c-

Si^M pillar with M=0.5 MSi and 5 MSi, respectively, it is in the same way for a-Si$^{0.5 \, MSi}$ pillar and a-Si$^{5 \, MSi}$ pillar. The corresponding SED spectrum only including the atoms in Si membrane is shown in Figure 4 (b). The SED spectrum including all atoms in the NPMs is shown in Figure S4 in the Supplementary Materials. For M=0.5 MSi, there are fewer vibrational modes in NPMs with crystalline and amorphous pillars compared with NPMs with M=MSi (Figure 2 (a), Type 3 and Type 4). In addition, the frequency of the first hybridization moves from 0.15 THz in Figure 2 (a) for Type 3 and Type 4 to ~0.2 THz in Figure 4 (a) for M=0.5 MSi. These phenomena imply that the local resonant hybridization should be weakened, which in turn results in a larger κ compared with NPM with M=MSi. For M=5 MSi, the frequency of the first hybridization moves to ~ 0.07 THz. However, the phonon dispersions from 0.7 to 1.4 THz are not severely changed as shown in Figure 4 (b), although the vibrational modes of the pillar are very dense. For the extreme case where M equals 5000 MSi, the SED, phonon dispersion and DOS are studied in Figure S6 in the Supplementary Materials.

3.3 The pillar height effect on the thermal conductivity of NPMs
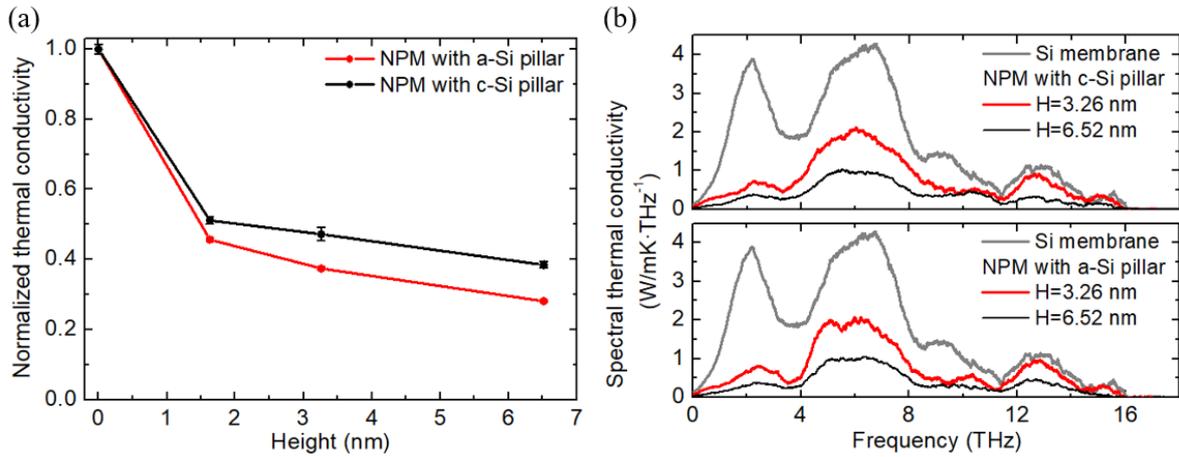
Figure 5 (a) Normalized thermal conductivity of NPM with c-Si pillar and a-Si pillar versus the height of pillars. (b) Spectral thermal conductivity of NPM with c-Si pillar and a-Si pillar for pillar heights of 3.26 nm and 6.52 nm.

Besides the different materials of pillars, the height (H) of pillars is another factor in tuning the κ of NPMs.[9] Here, the pillars with height of H =1.63, 3.26 and 6.52 nm are examined.

The κ of NPMs with c-Si pillar and a-Si pillar versus height are shown in Figure 5 (a). Further, the spectral κ of NPMs are calculated in Figure 5 (b). As shown in Figure 5 (a), the κ is largely reduced by 61% for c-Si pillar and 72% for a-Si pillar as the height increases to 6.52 nm, which is consistent with previous reports[13,36]. Moreover, the a-Si pillars cause larger reduction of κ than the corresponding c-Si pillar for each pillar height case. Further analyses show that the spectral κ of NPMs is reduced in the whole frequency range as the height of pillar increases.

4. Conclusions

In this work, the thermal conductivity of NPM with crystalline Si pillar, crystalline Ge pillar, and amorphous Si pillar are systematically investigated by MD simulations. The phonon dispersion and spectral energy density show that the phonon dispersions are flattened due to local resonant hybridization induced by both the crystalline pillar and the amorphous pillar. In addition, a-Si pillar can cause larger reduction of thermal conductivity compared with c-Si pillar. Moreover, the thermal conductivity of NPM with crystalline Si pillar is increased as the atomic mass of atoms in the pillar increases because of the weakened resonant hybridization. However, the thermal conductivity of NPM with amorphous Si pillar is almost unchanged as the atomic mass of atoms in the pillar increases. These results imply that the resonant hybridizations dominate the suppression of phonon transport in NPM with crystalline pillar, while the interface scatterings mainly contribute to the reduction of thermal conductivity of NPM with amorphous pillar. Further, the thermal conductivity of NPM is decreased as the pillar height increases for both crystalline pillar and amorphous pillar. The results of this work show that the thermal conductivity of NPMs can be tuned through the choice of pillar materials and heights for various applications requiring tailored thermal properties.

5. Acknowledgements

Reference

[1] J. Chen, X. Xu, J. Zhou, & B. Li, Interfacial thermal resistance: Past, present, and future. Reviews of Modern Physics **94**, 025002 (2022).

[2] C. Li, J. Wang, Y. Sheng, L. Yang, & Y. Su, The strain-dependent interfacial thermal resistance at graphene-silicon interface under various deformation conditions. International Journal of Heat and Mass Transfer **198**, 123383 (2022).

[3] Z. Tian, S. Lee, & G. Chen, Heat transfer in thermoelectric materials and devices. Journal of Heat Transfer **135**, 061605 (2013).

[4] Q. Yan & M.G. Kanatzidis, High-performance thermoelectrics and challenges for practical devices. Nature Materials **21**, 503 (2022).

[5] L. Yang, N. Yang, & B. Li, Thermoelectric properties of nanoscale three dimensional Si phononic crystals. International Journal of Heat and Mass Transfer **99**, 102 (2016).

[6] B.L. Davis & M.I. Hussein, Nanophononic metamaterial: Thermal conductivity reduction by local resonance. Physical Review Letters **112**, 055505 (2014).

[7] S. Xiong, K. Sääskilahti, Y.A. Kosevich, H. Han, D. Donadio, & S. Volz, Blocking phonon transport by structural resonances in alloy-based nanophononic metamaterials leads to ultralow thermal conductivity. Physical Review Letters **117**, 025503 (2016).

[8] K. Ren, X. Liu, S. Chen, Y. Cheng, W. Tang, & G. Zhang, Remarkable reduction of interfacial thermal resistance in nanophononic heterostructures. Advanced Functional Materials **30**, 2004003 (2020).

[9] M.I. Hussein, C.N. Tsai, & H. Honarvar, Thermal conductivity reduction in a nanophononic metamaterial versus a nanophononic crystal: A review and comparative analysis. Advanced Functional Materials **30**, 1906718 (2020).

[10] R. Anufriev, J. Maire, & M. Nomura, Review of coherent phonon and heat transport control in one-dimensional phononic crystals at nanoscale. APL Materials **9**, 070701 (2021).

[11] R. Anufriev & M. Nomura, Phonon and heat transport control using pillar-based phononic crystals. Science Technology of Advanced Materials **19**, 863 (2018).

[12] Z. Zhang, Y. Guo, M. Bescond, J. Chen, M. Nomura, & S. Volz, Heat conduction theory including phonon coherence. Physical Review Letters **128**, 015901 (2022).

[13] H. Honarvar & M.I. Hussein, Two orders of magnitude reduction in silicon membrane thermal conductivity by resonance hybridizations. Physical Review B **97**, 195413 (2018).

[14] L. Yang, N. Yang, & B. Li, Extreme low thermal conductivity in nanoscale 3D Si phononic crystal with spherical pores. Nano Letters **14**, 1734 (2014).

[15] M. Maldovan, Sound and heat revolutions in phononics. Nature **503**, 209 (2013).

[16] B.T. Spann, J.C. Weber, M.D. Brubaker, T.E. Harvey, L. Yang, H. Honarvar, C.-N. Tsai, A.C. Treglia, M. Lee, & M.I. Hussein, Semiconductor thermal and electrical properties decoupled by localized phonon resonances. Advanced Materials **35**, 2209779 (2023).

[17] R. Anufriev, R. Yanagisawa, & M. Nomura, Aluminium nanopillars reduce thermal conductivity of silicon nanobeams. Nanoscale **9**, 15083 (2017).

[18] J. Maire, R. Anufriev, T. Hori, J. Shiomi, S. Volz, & M. Nomura, Thermal conductivity reduction in silicon fishbone nanowires. Scientific Reports **8**, 4452 (2018).

[19] R. Anufriev & M. Nomura, Coherent thermal conduction in silicon nanowires with periodic wings. Nanomaterials **9**, 142 (2019).

[20] S. Neogi, J.S. Reparaz, L.F.C. Pereira, B. Graczykowski, M.R. Wagner, M. Sledzinska, A. Shchepetov, M. Prunnila, J. Ahopelto, & C.M. Sotomayor-Torres, Tuning thermal transport in ultrathin silicon membranes by surface nanoscale engineering. ACS nano **9**, 3820 (2015).

[21] X. Huang, D. Ohori, R. Yanagisawa, R. Anufriev, S. Samukawa, & M. Nomura, Coherent and incoherent impacts of nanopillars on the thermal conductivity in silicon nanomembranes. ACS applied materials & interface **12**, 25478 (2020).

[22] H. Zhang, B. Sun, S. Hu, H. Wang, Y. Cheng, S. Xiong, S. Volz, & Y. Ni, Novel phonon resonator based on surface screw thread for suppressing thermal transport of Si nanowires. Physical Review B **101**, 205418 (2020).

[23] D. Ma, X. Wan, & N. Yang, Unexpected thermal conductivity enhancement in pillared graphene nanoribbon with isotopic resonance. Physical Review B **98**, 245420 (2018).

[24] H. Wang, Y. Cheng, Z. Fan, Y. Guo, Z. Zhang, M. Bescond, M. Nomura, T. Ala-Nissila,

S. Volz, & S. Xiong, Anomalous thermal conductivity enhancement in low dimensional resonant nanostructures due to imperfections. Nanoscale **13**, 10010 (2021).

[25] A. Stukowski & engineering, Visualization and analysis of atomistic simulation data with OVITO–the Open Visualization Tool. Modelling Simulation in Materials Science **18**, 015012 (2010).

[26] J. Tersoff, Modeling solid-state chemistry: Interatomic potentials for multicomponent systems. Physical Review B **39**, 5566 (1989).

[27] A.P. Thompson, H.M. Aktulga, R. Berger, D.S. Bolintineanu, W.M. Brown, P.S. Crozier, P.J. in't Veld, A. Kohlmeyer, S.G. Moore, & T.D. Nguyen, LAMMPS-a flexible simulation tool for particle-based materials modeling at the atomic, meso, and continuum scales. Computer Physics Communications **271**, 108171 (2022).

[28] P.K. Schelling, S.R. Phillpot, & P. Keblinski, Comparison of atomic-level simulation methods for computing thermal conductivity. Physical Review B **65**, 144306 (2002).

[29] J.M. Larkin & A.J. McGaughey, Thermal conductivity accumulation in amorphous silica and amorphous silicon. Physical Review B **89**, 144303 (2014).

[30] I. Štich, R. Car, & M. Parrinello, Amorphous silicon studied by ab initio molecular dynamics: Preparation, structure, and properties. Physical Review B **44**, 11092 (1991).

[31] S. Tian, T. Wu, S. Hu, D. Ma, & L. Zhang, Boosting phonon transport across AlN/SiC interface by fast annealing amorphous layers. Applied Physics Letters **124** (2024).

[32] L. Yang, Y. Jiang, & Y. Zhou, Quantitatively predicting modal thermal conductivity of nanocrystalline Si by full-band Monte Carlo simulations. Physical Review B **104**, 195303 (2021).

[33] J.D. Gale & A.L. Rohl, The general utility lattice program (GULP). Molecular Simulation **29**, 291 (2003).

[34] J. Larkin, J. Turney, A. Massicotte, C. Amon, & A. McGaughey, Comparison and evaluation of spectral energy methods for predicting phonon properties. Journal of Computational Theoretical Nanoscience **11**, 249 (2014).

[35] J.A. Thomas, J.E. Turney, R.M. Iutzi, C.H. Amon, & A.J. McGaughey, Predicting phonon dispersion relations and lifetimes from the spectral energy density. Physical Review B **81**,

081411 (2010).

[36] H. Honarvar & M.I. Hussein, Spectral energy analysis of locally resonant nanophononic metamaterials by molecular simulations. Physical Review B **93**, 081412 (2016).

[37] Y. Zhou, X. Zhang, & M. Hu, Quantitatively analyzing phonon spectral contribution of thermal conductivity based on nonequilibrium molecular dynamics simulations. I. From space Fourier transform. Physical Review B **92**, 195204 (2015).

[38] Y. Xu, L. Yang, & Y. Zhou, The interfacial thermal conductance spectrum in nonequilibrium molecular dynamics simulations considering anharmonicity, asymmetry and quantum effects. Physical Chemistry Chemical Physics **24**, 24503 (2022).

[39] X. Li, K. Maute, M.L. Dunn, & R. Yang, Strain effects on the thermal conductivity of nanostructures. Physical Review B **81**, 245318 (2010).

[40] D.P. Sellan, E.S. Landry, J. Turney, A.J. McGaughey, & C.H. Amon, Size effects in molecular dynamics thermal conductivity predictions. Physical Review B **81**, 214305 (2010).

[41] J.-H. Lee, J. Grossman, J. Reed, & G. Galli, Lattice thermal conductivity of nanoporous Si: Molecular dynamics study. Applied Physics Letters **91**, 223110 (2007).

[42] C.J. Glassbrenner & G.A. Slack, Thermal conductivity of silicon and germanium from 3 K to the melting point. Physical Review **134**, A1058 (1964).